Solvation Dynamics of Electron Produced by Two-Photon Ionization of Liquid Polyols. III. Glycerol

J. Bonin,[†,‡,§] I. Lampre,[†,‡] P. Pernot,[†,‡] and M. Mostafavi*[,†,‡]

Laboratoire de Chimie Physique/ELYSE, Université Paris-Sud 11, UMR 8000, Bât. 349, Orsay, F-91405, France, and CNRS, Orsay, F-91405, France

Received: October 22, 2007; In Final Form: December 6, 2007

The solvation dynamics of excess electrons in glycerol have been measured by the pump−probe femtosecond laser technique at 333 K. The electrons are produced by two-photon absorption at 263 nm. The change in the induced absorbance is followed up to 450 ps in the spectral range from 440 to 720 nm. The transient signals of electron solvation have been analyzed by two kinetic models: a stepwise mechanism and a continuous relaxation model, using a Bayesian data analysis method. The results are compared with those previously published for ethylene glycol (*J. Phys. Chem. A* **2006**, *110*, 175) and for propanediols (*J. Phys. Chem. A* **2007**, *111*, 4902). From the comparison, it is pointed out that solvation dynamics in glycerol is very fast despite its high viscosity. This is interpreted as the existence of efficient traps for the electrons in glycerol with low potential energy. The small shift of the absorption band of the excess electron indicates that the potential of these traps is very close to that corresponding to the fully solvated electron.

1. Introduction

After the first experimental observation of the hydrated electron by microsecond pulse radiolysis measurements in 1962,[1] the challenge was to detect its formation dynamics. Due to the time resolution detection at that moment, the study of solvation dynamics of electrons was not examined in water but in alcohols, because of their high viscosity, their diversity and their low freezing point. Therefore, the first important results in solvation dynamics were obtained in alcohols at low temperature using a nanosecond pulse radiolysis setup.[2] It was shown that at short time the electron is partially solvated and that the solvation dynamics can be followed by time-resolved absorption spectroscopy. Later, with picosecond pulse radiolysis measurements, the existence of different states in solvation dynamics in alcohols were confirmed.[3,4] But the time resolution was still too poor to study electron solvation dynamics in water[5] or even to bring a whole picture on solvation dynamics of electrons in alcohols. Recently, femtosecond lasers and pump−probe techniques have provided astonishing insights in the solvation dynamics study of electrons in liquids. The first measurements were done in water, and it was clearly found that the electron is fully hydrated in less than a few picoseconds.[6] Since then, several studies have been conducted in water and methanol, with better time and spectral resolution.[7−21]

Despite these studies, several important questions remain open. For example: which are the intermediate species during the formation of the fully solvated electron? How is the structure of the solvent molecules involved in the solvation dynamics? Different studies have formulated various kinetic mechanisms for the solvation processes in water and in alcohols. Recently, our group contributed to that discussion by studying the solvation of electrons in a previously unstudied series of alcohols: the polyols.[22−27] High viscosity of polyols should slow down the solvation dynamics, and it also allows an easy formation of a liquid jet. In addition, the absorption spectrum of solvated electrons in these solvents is localized in the visible range. Finally, the use of polyols enables us to investigate the effect of molecular structure of the liquid on the solvation dynamics of electron by using different isomers of the same molecule. First of all, we have reported the study conducted in ethylene glycol (EG, 1,2-ethanediol).[26] We observed that at very short time delay after the pump pulse, the excess electron in EG, produced by two-photon ionization, presents a very broad absorption band in the visible and near-infrared domain with a maximum around 675 nm. The red part of the absorption band drops rapidly for the first five picoseconds while the blue part increases slightly, leading to a blue shift of the absorption band maximum down to 590 nm. Then, the absorbance on the red side of the spectrum follows its decrease while the absorbance on the blue side remains nearly constant. As a consequence, the maximum of the absorption band continues to shift toward shorter wavelengths and, 50 ps after the pump pulse, it is around 570 nm, i.e., the position of the absorption band maximum of the equilibrated solvated electron in EG. In a second work, we have studied the formation of solvated electrons in two neat isomers of propanediol (PD).[27] The excess electron in both propane-1,2-diol (12PD) and propane-1,3-diol (13PD) as in EG presents a wide absorption band in the visible and the near-IR at very short time delays after the pump pulse. The time-resolved spectra also revealed that a localized electron, which absorbs in the blue spectral domain, is quickly formed and relaxes to the equilibrated solvated electron in a couple of tens of picoseconds. For the EG case, we found it worthwhile to analyze our data with various approaches and we tested eleven models based on sequential stepwise mechanisms or continuous relaxation processes.[26] Four kinetic models gave a good quality fit of our spectrokinetic signals with a minimum number of adjustable parameters: a two-step model (STEP3), a heterogeneous (CRELH) or biexponential (CREX2) continuous relax-

* Corresponding author. E-mail: mehran.mostafavi@lcp.u-psud.fr.
† Université Paris-Sud 11.
‡ CNRS.
§ Present address: Laboratoire d'Electrochimie Moléculaire, Université Paris Diderot, Paris 7, 2 place Jussieu, 75251 Paris cedex 05, France.

10.1021/jp710203v CCC: $40.75
Published on Web 02/12/2008

ation model, and a modified hybrid model with a stepwise transition followed by a homogeneous continuous relaxation (HYBM). Taking into account those results, for the data in PD, we have retained the first three models, the simplest ones. Interesting results have been obtained for 12PD and 13PD, which have almost the same viscosity at room temperature (40 and 39 cP, respectively). Even if the electron is better trapped in 12PD just after the pump pulse, from the analysis, the spectral evolution appears faster for 13PD than for 12PD, indicating the faster solvation process in 13PD compared to 12PD. The slower solvation dynamics corresponds to the vicinal diol. That suggests greater molecular changes in close proximity to the electron site, which have longer range effects. For instance, that may indicate a different number of first solvation shell molecules, insofar as only one or both of the OH-groups of the diol molecule may be involved in the electron cavity.

In this work, we present the results obtained on the solvation dynamics of electron in glycerol (GLY, propane-1,2,3-triol) using femtosecond pump−probe optical absorption measurements. The molecular structure of this highly viscous solvent having a high hydrogen bond density contains three hydroxyl groups in the vicinity and completes the series of polyols previously studied. Very soon after the observation of hydrated electrons, pulse radiolysis experiments were performed at very low temperature in glasses using glycerol as pure liquid or in mixtures.[28−30] The absorption spectrum of the solvated electron in pure GLY was measured at different temperatures: a red shift of the spectrum with increasing temperature from 76 to 305 K was described.[31−33] Recently, the spectrum of the solvated electron in glycerol, generated by photodetachment from a halogen anion, between 329 and 536 K has been reported.[34] From different results obtained by changing the solvent temperature, it appears that the shift of the absorption spectrum of the fully solvated electron is more important in PD than in EG and in GLY.[22,24,34]

In the present work, the experiments with GLY were performed at 333 K to make it possible to form the liquid jet used as sample. Even at this temperature the viscosity of GLY is higher (76 cP) than that of PD at room temperature (40 and 39 cP for 12PD and 13PD, respectively). Hereafter, the solvation dynamics of electron in GLY is detailed and compared with those in EG and in PD and the effect of the molecular structure of the liquid is discussed.

2. Experimental and Data Analysis Methods

2.1. Experimental Section. The apparatus and procedures have already been described in detail in paper I.[26] Briefly, the output of an amplified kilohertz femtosecond Ti:sapphire laser system (Spectra Physics) was split into two parts to generate the pump and probe pulses. The pump beam at 263 nm was produced by frequency doubling and sum-frequency mixing in two BBO crystals of 90% of the fundamental beam. The pump beam was then focused on a 300 μm thick liquid jet in order to produce electrons by photoionization of the solvent. The remaining 10% of the fundamental beam at 790 nm was directed to a variable optical delay line and focused on a 3 mm sapphire disk to generate a white-light continuum. The continuum beam was divided into a probe and a reference beam by a broad band beam-splitter. The probe beam was focused onto the liquid jet sample. Then, the probe beam was dispersed on a polychromator and detected on a CCD camera (Princeton Instruments) with a resolution of 0.2 nm per pixel, simultaneously with the reference beam to take into account any laser fluctuations. Time-resolved spectra were recorded from 440 to 720 nm and corrected for the group velocity dispersion.

As depicted earlier, the transient absorption signals recorded at wavelengths below 600 nm exhibit a sharp "spike" at the time origin (the "coherent artifact") due to nonlinear absorption of the pump and probe light in the sample.[6,16,18,26,35,36]

Glycerol from Aldrich (ACS Reagent) was used without further purification. The experiments were performed at 333 K because, due to the viscosity of glycerol at 295 K (around 1000 cP), it was not possible to form a solvent jet at room temperature with our circulating system. We heated the container of the glycerol at around 353 K, but, due to the solvent circulation, the temperature of the solvent decreases. Then, the temperature of the probed sample was measured in the jet with a thermocouple and found to be 333 K. At this temperature, the viscosity of the solvent decreases to 76 cP[37] and makes possible the formation of a liquid jet.

2.2. Data Analysis. As in the previous works, for all the kinetic models, the "coherent artifact" around the zero time delay is described by a time-symmetric combination of three generalized Gaussian functions:

$$\begin{aligned} A_0(t,E) = &-a_1(E)\,\mathscr{G}(t;t_0(E)-\Delta,\gamma_1,\alpha) \\ &+ a_2(E)\,\mathscr{G}(t;t_0(E),\gamma_2,\alpha) \\ &- a_3(E)\,\mathscr{G}(t;t_0(E)+\Delta,\gamma_1,\alpha) \end{aligned} \quad (1)$$

with

$$\mathscr{G}(t;t_0,\gamma,\alpha) = \exp\left(-\left|\frac{t-t_0}{\gamma}\right|^{\alpha}\right) \quad (2)$$

where $\alpha \geq 2$, and $t_0(E)$ corresponds to the group velocity dispersion curve in energy space.

For the sequential stepwise relaxation cascades, only the two-step mechanism with three species (STEP3P) has been considered to account for the electron solvation in GLY. Each considered species or state of the excess electron is supposed to have a fixed and individual spectrum. The time-dependent absorbance is then written

$$A(t,E) = A_0(t,E) + \mathscr{G}(t;t_0(E),\sigma/\sqrt{4\ln 2},2) \otimes \sum_{k=1}^{3} c_k(t)\,\epsilon_k(E) \quad (3)$$

where $\mathscr{G}(t;t_0(E),\sigma/\sqrt{4\ln 2},2)$ represents the instrumental response function (cross correlation of the pump and probe pulses) and the $\otimes$ symbol stands for the convolution operator. The concentration curves $c_k(t)$ are obtained analytically by the standard Laplace transform method. The absorption spectra of excess electron have been modeled by a lognormal shape function S:

$$\epsilon_k(E) = \epsilon_k S(E;E_{\max,k},\Omega_k,\gamma_k) \quad (4)$$

where S is parametrized by the peak position $E_{\max}$, the full width at half-maximum Ω and the asymmetry factor γ. The value of the extinction coefficient at the maximum of the fully solvated electron in GLY is assumed to be 10500 L mol^{-1} cm^{-1} as suggested by Jay-Gerin et al. from the values of the radiolytic yield of the solvated electron.[38] This value is lower than that usually reported of 12000 L mol^{-1} cm^{-1}. But according to our measurements with pulse radiolysis in the case of PD[25] and according to the results in EG,[26] we assume that the lower value of the extinction coefficient is more accurate. Lognormal analysis of the absorption spectrum of the fully solvated electron provides shape parameters ($E_{\max}$, Ω and γ, see Table 1) in agreement with those reported in the literature.[34]

TABLE 1: Parameters of the STEP3P Model Resulting from the Probabilistic Analysis of the Experimental Data for the Solvation of Electron in Glycerol at 333 K

parameter	e^-_{wb}	e^-_{sb}	e^-_s
ϵ (M^{-1} cm^{-1})	10200 ± 140	11280 ± 130	10500
E_{max} (eV)	2.00 ± 0.02	2.22 ± 0.05	2.28
Ω (eV)	1.78 ± 0.05	1.34 ± 0.02	1.35
γ	1.58 ± 0.2	1.63 ± 0.04	1.50
τ (ps)	2.6 ± 0.3	14.9 ± 1.4	

Models of continuous spectral evolution where the time-dependent absorption spectrum of a unique species is described by a lognormal function with time-dependent coefficients have also been tested:

$$A(t,E) = A_0(t,E) + \mathcal{G}(t;t_0(E),\sigma/\sqrt{4\ln 2},2) \otimes [c_0\epsilon(t) \times S(E;E_{max}(t),\Omega(t),\gamma(t))] \quad (5)$$

To account for the presence of various solvation sites and/or relaxation rates heterogeneity, the time-dependence of each parameter ($x = \epsilon$, E_{max}, Ω, γ) is modeled by a biexponential function (CREX2):

$$x(t) = x_\infty + \Delta_{x,1}\mathcal{G}(t;0,\tau_{x,1},1) + \Delta_{x,2}\mathcal{G}(t;0,\tau_{x,2},1) \quad (6)$$

The complete description of our data analysis method, including data conditioning, Bayesian data analysis and model selection is given in papers I and II. We performed the global analysis of the 2D spectrokinetic data matrix **D** obtained by pump−probe measurements in GLY to determine the kinetic and spectral parameters involved in the general expression for the transient absorbance:

$$D_{ij} \cong A(t_i,E_j) \quad (7)$$

3. Results and Discussion

As it is known that electrons generated in different photoprocesses have different thermalization and geminate recombination dynamics, it is important to identify whether the ionization of GLY proceeds via a two- or three-photon excitation.[12,39] The ionization threshold of liquid GLY is known to be 8.1 ± 0.1 eV.[40] Consequently, the energy of 263 nm photons being 4.7 eV, the ionization of liquid GLY should occur by a two-photon absorption mechanism. Therefore, we checked the mechanism by measuring the transmittance of the 300 μm liquid jet versus the peak power of the 263 nm input pulse.

The transmittance evolution is clearly characterized by a single-beam two-photon absorption mechanism at 263 nm (Figure 1).[41−43] In that case, the measured transmittance (T) corresponding to the ratio of the transmitted pulse energy E to the incident pulse energy E_0 is given by

$$T = \frac{E}{E_0} = \frac{(1-R)^2}{E_0}\int_0^\infty dr\, 2\pi r \int_{-\infty}^{\infty} dt \frac{I_0(r,t)}{[1+\beta L(1-R)I_0(r,t)]} \quad (8)$$

where R represents the Fresnel reflection losses at the air−liquid jet interfaces and L is the jet thickness. We have fitted our experimental values of the transmittance (T) as a function of the peak irradiance (I_0) with eq 8, and we have determined the values of β and R. We find that $\beta = (3.5 \pm 0.5) \times 10^{-11}$ m W^{-1} and $R = 0.06$. These values of β and R are slightly higher than the values obtained for EG, 12PD and 13PD at 263 nm. The surface roughness of the jet inducing additional scattering can account for the larger value of R compared to the value calculated with the refractive index.

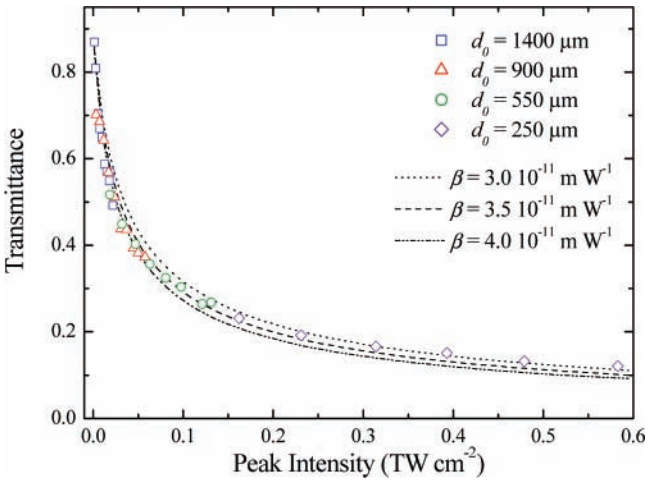

Figure 1. Transmittance of the 300 μm jet of liquid glycerol jet at 333 K *versus* the peak intensity of the 220 fs pump pulse at 263 nm (symbols, experimental data for four different beam diameters; lines, calculated curves using eq 8 for three different values of β and $R = 0.06$).

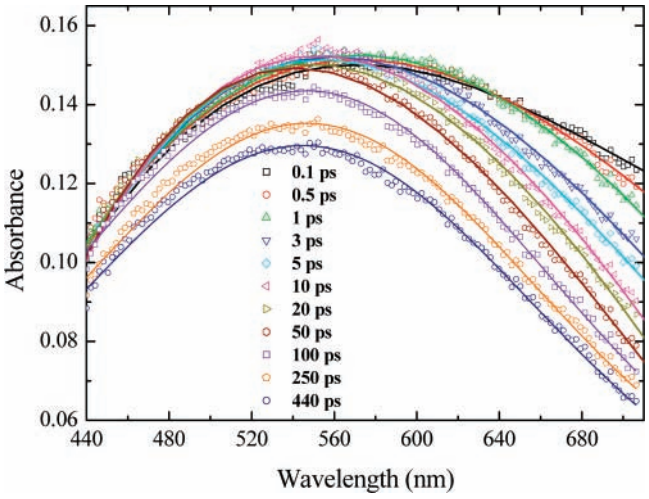

Figure 2. Time evolution of the absorption spectrum upon two-photon ionization of liquid glycerol at 263 nm. Solid lines through experimental points are guides for the eyes.

The evolution of the absorption spectrum is reported in Figure 2. Even at very short time after the laser pump pulse, no significant contribution in the near-IR is observed. The maximum of the absorption is around 580 nm, very close to the maximum of the absorption spectrum of the fully solvated electron in GLY at 333 K (located around 545 nm). Our experimental value for the maximum of the absorption band at 333 K is slightly lower than the 555 nm reported recently by Chandrasekhar et al.,[34] but stands within the experimental uncertainties. The shift of the absorption spectrum maximum is important in the first ten picoseconds. From 1 ps to around 100 ps, a decrease in the red part of the absorption spectrum occurs without any significant change in the blue part. After 100 ps, the intensity of the whole transient absorption band decreases due to the geminate recombination. Nevertheless, due to the high viscosity of this solvent, even at 333 K, geminate recombination is very slow, and 450 ps after the laser pulse, less than 15% of the intensity of the absorbance of the fully solvated electron is lost.

The kinetics for three different wavelengths are reported in Figure 3. At 700 nm a fast decay is followed by a slower one. At 560 nm, a fast increase of the signal is observed for the first 2 ps, followed by a slower rise until 15 ps, and after by a slow

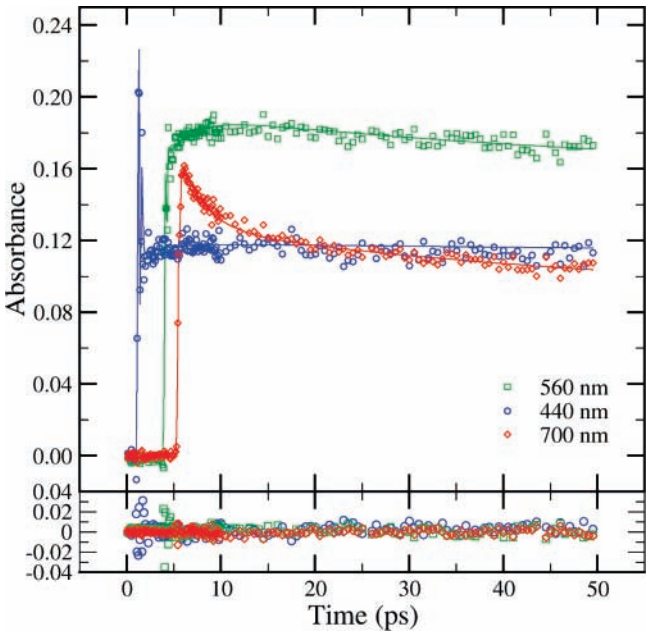

Figure 3. Transient absorption signals at three representative wavelengths obtained upon 263 nm photoionization of liquid glycerol. Open symbols represent experimental data not corrected for the group velocity dispersion for clarity reasons. Solids lines correspond to the best global fit obtained with the STEP3P mechanism, and the bottom window contains the fit residues.

continuous decay. Finally, at 440 nm in the blue side of the spectral window, a slight increase of the absorbance is observed during the first 15 ps and then again a slow decay takes place, as in the case of 700 and 560 nm.

It is to be noted that the "coherent artifact" in this solvent is different from that reported for the PD and EG and affects more strongly the signals during the first 500 fs. The difference could be due to the higher refractive index of GLY compared to those of EG and PD.

We fit our data by two kinetic models. First, a stepwise mechanism involving three species (weakly bound e^-_{wb}, strongly bound e^-_{sb} and fully solvated electron e^-_s) is used. This kinetic model (STEP3P) is very common and gives a simple picture of solvation dynamics as shown in our previous papers. Second, a continuous relaxation model (CREX2) is applied. This model considers only one species with an absorption band spectrum evolving continuously in position and shape. The latter using a biexponential function for each optimized parameter (ϵ, E_{max}, Ω and γ) is more efficient and gave us the best fit of the data for EG and PD.

The three-state model (STEP3P) provides a good fit of our experimental data for GLY. The optimal spectra and kinetics of the three species are displayed in Figure 4, and the values of the parameters are reported in Table 1.

According to the stepwise model, the weakly bound electron, e^-_{wb}, converts into the intermediate species, e^-_{sb}, with a time constant τ_1 of about 2.6 ps (Figure 4a). The strongly bound, e^-_{sb}, gives very slowly the solvated electron, e^-_s, with a time constant τ_2 around 14.9 ps. The value of τ_1 obtained for GLY is lower than those determined for both PD (4.5 and 3.2 ps for 12PD and 13PD, respectively) and slightly larger than the value found for EG (1.3 ps). The value of τ_2 (14.9 ps) is lower than those found for 12PD (54.6 ps), 13PD (34.6 ps) and EG (25 ps). This result cannot be explained by the respective values of the viscosity of the different polyols, as the viscosity of GLY is the highest but the kinetics of electron solvation is the fastest.

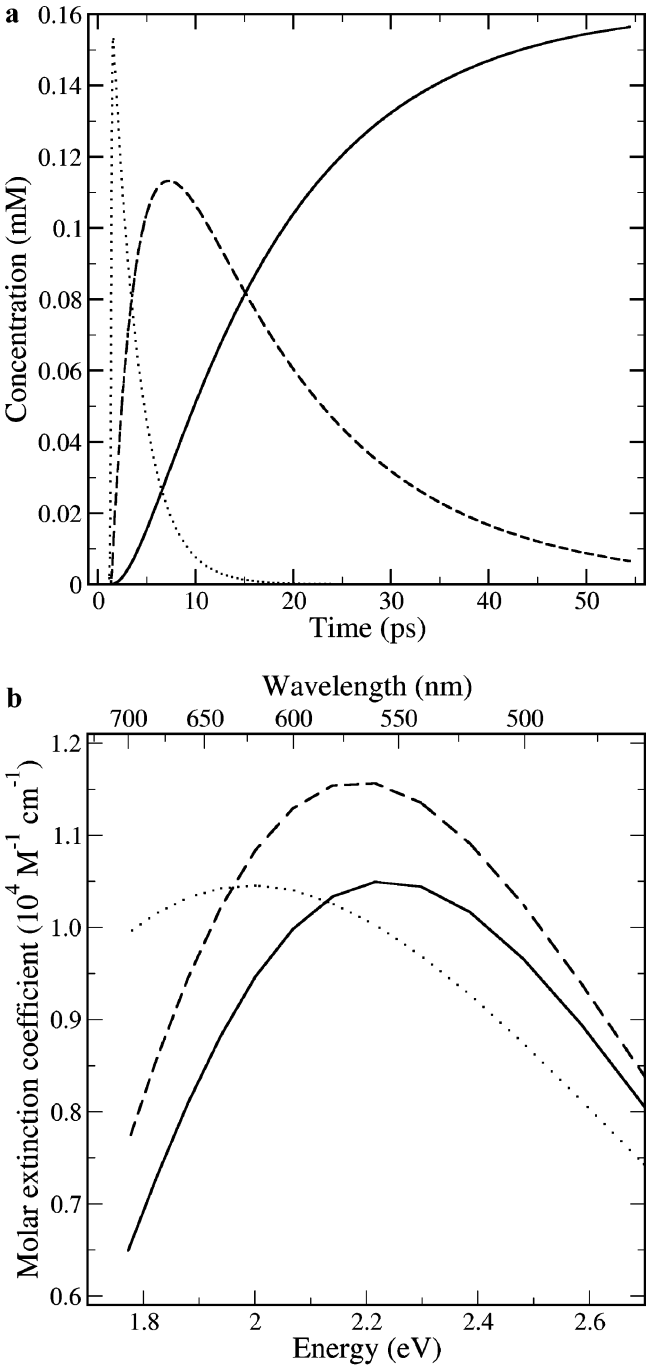

Figure 4. (a) Time evolution of the concentrations and (b) absorption spectra of the three species involved in the stepwise mechanism (STEP3P) used to fit the experimental data: (•••) e^-_{wb}, (− − −) e^-_{sb} and (—) e^-_s.

The absorption spectra of the three species involved in the STEP3P model are shown in Figure 4b. The first species (e^-_{wb}), which appears after solvent ionization by two-photon absorption, presents an absorption band in the visible domain with a maximum at 625 nm. It is interesting to note that in the case of 12PD and 13PD the maximum of absorption of this species is located outside of the observation window in the near-IR. The second species (e^-_{sb}) shows a broad absorption band with a maximum around 570 nm. This band is close to that of the fully solvated electron e^-_s, in the blue side of the spectrum. It is to be noted that the shape and the position of the absorption band of the weakly bound electron compared to the shape of the absorption band of the same species in PD highlight a very quick

TABLE 2: Parameters of the CREX2 Model Resulting from the Probabilistic Analysis of the Experimental Data for the Solvation of Electron in Glycerol 333 K

x	x_∞	Δ_{x1}	τ_{x1} (ps)	Δ_{x2}	τ_{x2} (ps)
ϵ (M^{-1} cm^{-1})	10500	4000 ± 700	230 ± 30		
E_{max} (eV)	2.28	-2.28 ± 0.03	0.16 ± 0.01	-0.12 ± 0.01	8.2 ± 0.2
Ω (eV)	1.35	1.5 ± 0.2	0.01 ± 0.001	0.38 ± 0.03	2.27 ± 0.05
γ	1.5	0		0	

TABLE 3: Comparison of Characteristic Times for the Solvation of Electron in Four Polyols Using the CREX2 Model

solvent:		EG	12PD	13PD	GLY
viscosity (cP):		16	40	39	76
OH-density (mol L^{-1}):		35.7	27.1	27.7	41.2
E_{max}	$\tau_{E_{max1}}$ (ps)	1.7	0.6	0.2	0.16
	$\tau_{E_{max2}}$ (ps)	25.5	27.5	20.6	8.2
Ω	$\tau_{\Omega_{max1}}$ (ps)	1.7	1.0	2.6	0.01
	$\tau_{\Omega_{max2}}$ (ps)	25.5	76.0	40.5	2.27

formation of well-localized electrons and suggests the presence of pre-existing traps in GLY.

We have also performed a fit of our spectrokinetic data considering a time-dependent absorption spectrum of a unique species. The time dependence of the spectral parameters is described by biexponential functions (CREX2) as done previously.[26,27] The results are reported in Table 2. Fits of the data are better than in the case of the STEP3P model. In fact, the value of the Bayes information criterion (I_B), which is an index of model performance, is higher for CREX2 than for STEP3P, and the value of the root-mean-square (rms) is 4.5×10^{-3} and 4.07×10^{-3} for STEP3P and CREX2 models respectively.

From the parameters involved in the CREX2 model, the relaxation times are 0.16 and 8.2 ps for the E_{max}. The first relaxation time, faster than in other diols (Table 2), is too fast (160 fs), compared to our time resolution, and it is not reliable. Indeed, the intensity of the signal due to the cross correlation of the pump and probe pulses, the "coherent artifact", is important and it strongly affects the signal within the first 500 fs. That means that the value of $\Delta E_{max} = -2.28 \pm 0.03$ eV derived from CREX2 model is biased (Table 2). Nevertheless, these results clearly indicate that the shift of the absorption band to 560 nm occurs with a relaxation time of 8.2 ps, which is shorter than the time constants found in the cases of PD and EG. For the width of the absorption band, a similar behavior is found, the relaxation times being 0.01 and 2.27 ps. As we pointed out, the first value is biased. The values of the asymmetry factor γ were quite dispersed and not well-defined in the case of 12PD and 13PD, especially at short time, because the transient absorption spectra exhibit a very broad absorption band in the visible but also the near-IR domain, out of our experimental spectral window. In the case of GLY, the asymmetry factor is well-defined and does not change with time. In addition, the extinction coefficient of the absorption band is almost constant in the case of GLY. From the time-dependent width and asymmetry factor of the absorption band, we can deduce that the absorption band of excess electron in GLY quickly reaches a stabilized form.

The different characteristic times obtained with the CREX2 model for the different polyols are summed up in Table 3. Figure 5 depicts the time evolution of the maximum and width of the absorption band deduced from the CREX2 model, along with the experimental data for the different polyols from 500 fs (to avoid the effect of the "coherent artifact") up to 100 ps. First, it is to be noticed that the CREX2 model fits remarkably well the experimental data, especially for glycerol. Then, in spite of

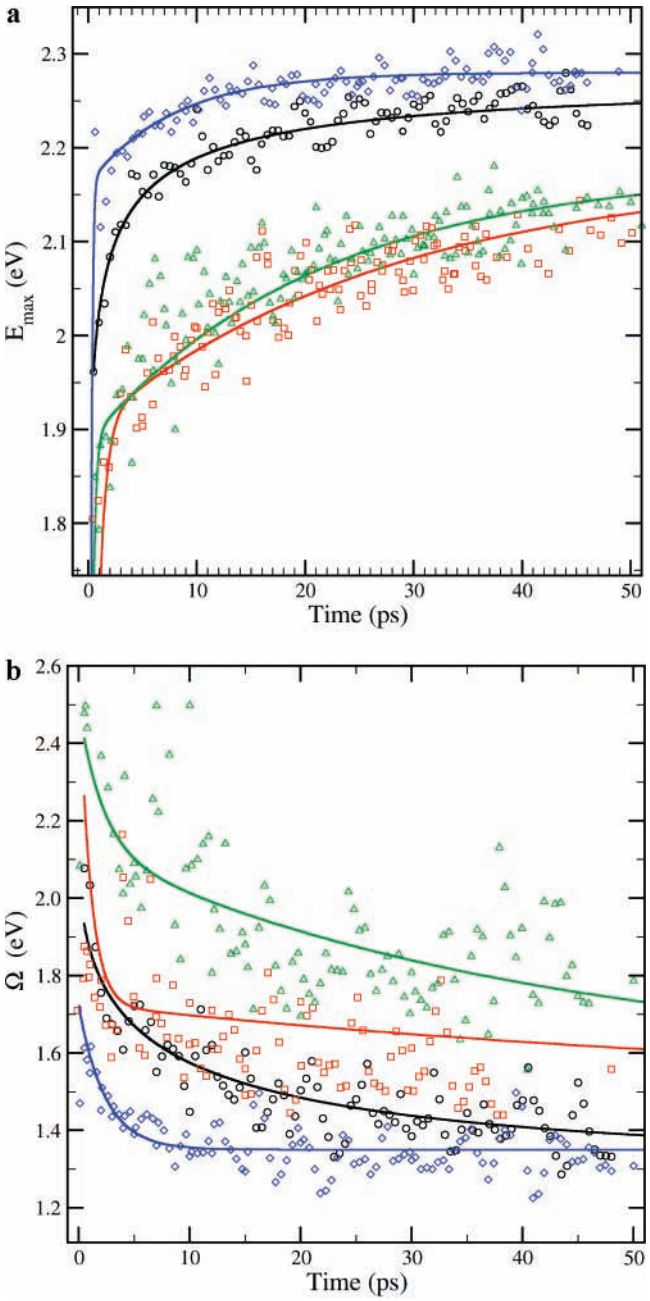

Figure 5. Time evolution of (a) the peak position E_{max} and (b) the width Ω of the absorption band of the photogenerated excess electron in the four studied polyols. The open symbols (blue ◇ GLY, black ○ EG, green △ 13PD and red □ 12PD) correspond to the parameters of the lognormal function fitting individually each experimental spectrum from 500 fs to 50 ps. The solid lines correspond to the global fit of the experimental data obtained by the CREX2 model.

the higher viscosity of GLY at 333 K than the viscosity of PD at room temperature, we observe that the solvation dynamics is faster in GLY than in PD. Even compared with EG, the position of the maximum of the absorption band of the fully solvated electron is reached much faster in the case of GLY. A similar behavior is observed for the time evolution of the

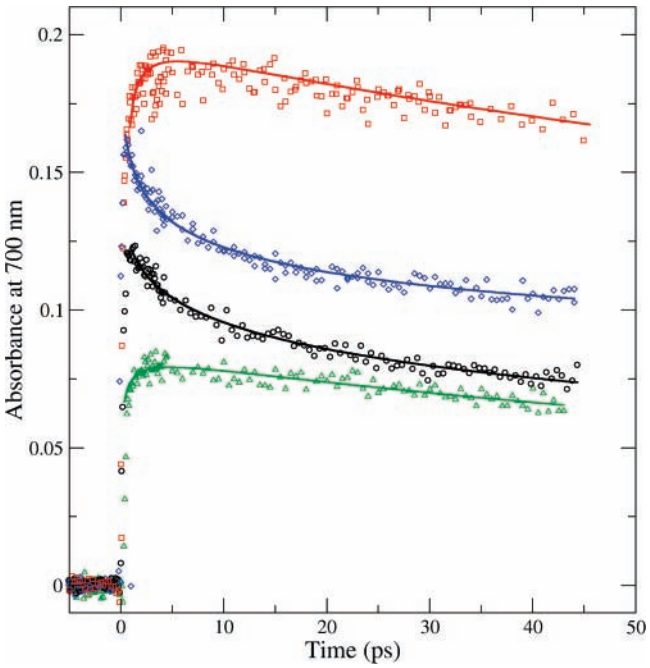

Figure 6. Transient absorption signals at 700 nm recorded after photoionization of the four different polyols blue ◇ GLY, black ○ EG, green △ 13PD and red □ 12PD.

bandwidth which reaches the value of that of the fully solvated electron much more rapidly for GLY (roughly 10 ps) than for other polyols. The change in the shape of the absorption band of the excess electron in the polyols versus time mainly occurs in the red side of the spectra. The kinetics observed for the 4 polyols at 700 nm (Figure 6) shows only a decay in the case of EG and GLY but a rise followed by a decay for PD, and confirms that the decay is very fast in the case of GLY compared to those in the three other polyols.

These results clearly demonstrate that the solvation dynamics in the polyols depends on the molecular structure of the solvent and cannot be explained by the viscosity alone. In their theoretical works, Abramczyk and co-workers as well as Hilczer and co-workers had pointed out the importance of the coupling between the excess electron and the intramolecular modes of the solvent on the absorption band of the excess electron in both the visible and near-IR domains. They considered that the dynamics of the solvated electron is mainly governed by the vibrational properties of matrices in which the electron is trapped.[44,45] Recent results on resonance Raman experiments performed by Tauber and Mathies support this description.[46,47] Two kinds of trapped electrons are proposed in alcohols: visible absorbing electrons associated with the hydroxyl traps (coupling with the bending mode C−OH) and IR-absorbing electrons trapped in the alkyl group (coupling with the C−H stretching modes). Distinction between the two kinds of trapped electrons was earlier indicated by several authors.[3,48−50] The existence of two kinds of traps, respectively where the paraffinic and the hydroxyl groups are locally concentrated, had been evidenced at 77 K only for monohydroxy-alcohols and not for polyhydroxy-alcohols, indicating that, in the latter solvents, the phase is not segregated into polar and nonpolar regions owing to the abundance of the H-bonds.[51] Consequently, we can consider that the time evolution of the spectral profiles of excess electrons in GLY is also related to vibronic coupling and vibrational relaxation in the first-solvation shell molecules. The fact that even at very short time no absorption band in the near-IR is observed indicates that the electron is mostly associated with the hydroxyl traps, which is reasonable due to the high OH group density in the case of GLY. Moreover, the similarities observed for the evolution of E_{max} (Figure 5a) in EG and GLY on the one hand and 12PD and 13PD on the other hand must be related to the OH-group density (Table 3).

4. Conclusion

The time-dependent absorption band of the photogenerated excess electron in glycerol was observed using a femtosecond pump−probe setup. The excess electrons were produced by two-photon absorption in neat glycerol at 333 K. The analysis of the spectrokinetic measurements shows that the electron solvation dynamics in this solvent can be modeled either by a stepwise mechanism involving two species or a continuous relaxation one with biexponential functions. The results show that the excess electron is very quickly trapped and fully solvated. The small blue shift of the absorption band versus time highlights that the potential energy of the traps in glycerol is very close to that of fully solvated electron. This effect is attributed to the fact that liquid glycerol presents a very high hydroxyl group density.

References and Notes

(1) Hart, E. J.; Boag, J. W. *J. Am. Chem. Soc.* **1962**, *84*, 4090.
(2) Baxendale, J. H.; Wardman, P. *Nature* **1971**, *230*, 449.
(3) Chase, W. J.; Hunt, J. W. *J. Phys. Chem.* **1975**, *79*, 2835.
(4) Kenney-Wallace, G.; Jonah, C. D. *J. Phys. Chem.* **1982**, *86*, 2572.
(5) Rentzepis, P. M.; Jones, R. P.; Jortner, J. *J. Chem. Phys.* **1973**, *59*, 766.
(6) Migus, A.; Gauduel, Y.; Martin, J. L.; Antonetti, A. *Phys. Rev. Lett.* **1987**, *58*, 1559.
(7) Gauduel, Y.; Pommeret, S.; Migus, A.; Antonetti, A. *J. Phys. Chem.* **1989**, *93*, 3880.
(8) Pépin, C.; Goulet, T.; Houde, D.; Jay-Gerin, J.-P. *J. Phys. Chem.* **1994**, *98*, 7009.
(9) Shi, X.; Long, F. H.; Lu, H.; Eisenthal, K. B. *J. Phys. Chem.* **1995**, *99*, 6917.
(10) Walhout, P. K.; Alfano, J. C.; Kimura, T.; Silva, C.; Reid, P. J.; Barbara, P. F. *Chem. Phys. Lett.* **1995**, *232*, 135.
(11) Crowell, R. A.; Bartels, D. M. *J. Phys. Chem.* **1996**, *100*, 17940.
(12) Reuther, A.; Laubereau, A.; Nikogosyan, D. N. *J. Phys. Chem.* **1996**, *100*, 16794.
(13) Silva, C.; Walhout, P. K.; Yokoyama, K.; Barbara, P. F. *Phys. Rev. Lett.* **1998**, *80*, 1086.
(14) Yokoyama, K.; Silva, C.; Son, D. H.; Walhout, P. K.; Barbara, P. F. *J. Phys. Chem. A* **1998**, *102*, 6957.
(15) Assel, M.; Laenen, R.; Laubereau, A. *J. Chem. Phys.* **1999**, *111*, 6869.
(16) Goulet, T.; Pépin, C.; Houde, D.; Jay-Gerin, J.-P. *Radiat. Phys. Chem.* **1999**, *54*, 441.
(17) Thomsen, C. L.; Madsen, D.; Keiding, S. R.; Thogersen, J.; Christiansen, O. *J. Chem. Phys.* **1999**, *110*, 3453.
(18) Kloepfer, J. A.; Vilchiz, V. H.; Lenchenkov, V. A.; Germaine, A. C.; Bradforth, S. E. *J. Chem. Phys.* **2000**, *113*, 6288.
(19) Son, D. H.; Kambhampati, P.; Kee, T. W.; Barbara, P. F. *Chem. Phys. Lett.* **2001**, *342*, 571.
(20) Scheidt, T.; Laenen, R. *Chem. Phys. Lett.* **2003**, *371*, 445.
(21) Thaller, A.; Laenen, R.; Laubereau, A. *J. Chem. Phys.* **2006**, *124*, 024515/1.
(22) Mostafavi, M.; Lin, M.; He, H.; Muroya, Y.; Katsumura, Y. *Chem. Phys. Lett.* **2004**, *384*, 52.
(23) Soroushian, B.; Lampre, I.; Pernot, P.; De Waele, V.; Pommeret, S.; Mostafavi, M. *Chem. Phys. Lett.* **2004**, *394*, 313.
(24) Lampre, I.; Lin, M.; He, H.; Han, Z.; Mostafavi, M.; Katsumura, Y. *Chem. Phys. Lett.* **2005**, *402*, 192.
(25) Lin, M.; Mostafavi, M.; Muroya, Y.; Han, Z.; Lampre, I.; Katsumura, Y. *J. Phys. Chem. A* **2006**, *110*, 11404.
(26) Soroushian, B.; Lampre, I.; Bonin, J.; Pernot, P.; Mostafavi, M. *J. Phys. Chem. A* **2006**, *110*, 1705.
(27) Bonin, J.; Lampre, I.; Pernot, P.; Mostafavi, M. *J. Phys. Chem. A* **2007**, *111*, 4902.
(28) Ershov, B. G. *Indian J. Chem.* **1966**, *4*, 494.
(29) Ershov, B. G.; Makarov, I. E.; Pikaev, A. K. *Khim. Vys. Energ.* **1967**, *1*, 404.
(30) Ekstrom, A.; Willard, J. E. *J. Phys. Chem.* **1968**, *72*, 4599.
(31) Arai, S.; Sauer, M. C. *J. Chem. Phys.* **1966**, *44*, 2297.

(32) Kajiwara, T.; Thomas, J. K. *J. Phys. Chem.* **1972**, *76*, 1700.
(33) Jou, F. Y.; Freeman, G. R. *Can. J. Chem.* **1979**, *57*, 591.
(34) Chandrasekhar, N.; Krebs, P.; Unterreiner, A. N. *J. Chem. Phys.* **2006**, *125*, 164512/1.
(35) Ekvall, K.; van der Meulen, P.; Dhollande, C.; Berg, L.-E.; Pommeret, S.; Naskrecki, R.; Mialocq, J.-C. *J. Appl. Phys.* **2000**, *87*, 2340.
(36) Lorenc, M.; Ziolek, M.; Naskrecki, R.; Karolczak, J.; Kubicki, J.; Maciejewski, A. *Appl. Phys. B: Lasers Opt.* **2002**, *74*, 19.
(37) Sheely, M. L. *Ind. Eng. Chem.* **1932**, *24*, 1060.
(38) Jay-Gerin, J. P.; Ferradini, C. *J. Chim. Phys. PCB* **1994**, *91*, 173.
(39) Nikogosyan, D. N.; Oraevsky, A. A.; Rupasov, V. I. *Chem. Phys.* **1983**, *77*, 131.
(40) Jung, J.-M. Research Habilitation Report, Université Louis Pasteur - Strasbourg 1, 2003.
(41) Shen, Y. R. *The Principles of Nonlinear Optics*; Wiley: New York, 1984.
(42) Sutherland, R. L. *Handbook of Nonlinear Optics*; Dekker: New York, 1996.
(43) Pommeret, S.; Gobert, F.; Mostafavi, M.; Lampre, I.; Mialocq, J.-C. *J. Phys. Chem. A* **2001**, *105*, 11400.
(44) Abramczyk, H.; Werner, B.; Kroh, J. *J. Phys. Chem.* **1992**, *96*, 9674.
(45) Hilczer, M.; Steblecka, M. *Radiat. Phys. Chem.* **2003**, *67*, 263.
(46) Tauber, M. J.; Mathies, R. A. *J. Am. Chem. Soc.* **2003**, *125*, 1394.
(47) Tauber, M. J.; Stuart, C. M.; Mathies, R. A. *J. Am. Chem. Soc.* **2004**, *126*, 3414.
(48) Ogasawara, M.; Shimizu, K.; Yoshida, H. *Radiat. Phys. Chem.* **1981**, *17*, 331.
(49) Ogasawara, M.; Shimizu, K.; Yoshida, K.; Kroh, J.; Yoshida, H. *Chem. Phys. Lett.* **1979**, *64*, 43.
(50) Shida, T.; Iwata, S.; Watanabe, T. *J. Phys. Chem.* **1972**, *76*, 3683.
(51) Shida, T.; Iwata, S.; Watanabe, T. *J. Phys. Chem.* **1972**, *76*, 3691.